

1  
2  
3 **Potassium isotopic composition of various samples using a dual-path collision cell-**  
4 **capable multiple-collector inductively coupled plasma mass spectrometer, Nu**  
5 **Instruments Sapphire**  
6

7 Frédéric Moynier<sup>1</sup>, Yan Hu<sup>1</sup>, Kun Wang<sup>2</sup>, Ye Zhao<sup>3</sup>, Yvan Gérard<sup>3</sup>, Zhengbin Deng<sup>1</sup>,  
8 Julien Moureau<sup>1</sup>, Weiqiang Li<sup>4</sup>, Justin I. Simon<sup>5</sup>, Fang-Zhen Teng<sup>6</sup>  
9

10 <sup>1</sup>Institut de Physique du Globe de Paris, Université de Paris, CNRS, 1 rue Jussieu, Paris  
11 75005, France.

12 <sup>2</sup>Department of Earth and Planetary Sciences, Washington University in St. Louis, St  
13 Louis, MO 63130, USA.

14 <sup>3</sup>Nu Instruments, Unit 74 Clywedog Road South Wrexham Industrial Estate, Wrexham,  
15 LL13 9X, United Kingdom.

16 <sup>4</sup>School of Earth Sciences, Nanjing University, Nanjing, China.

17 <sup>5</sup>Center for Isotope Cosmochemistry and Geochronology, Astromaterials Research and  
18 Exploration Science division, NASA Johnson Space Center, Houston, TX 770058, USA.

19 <sup>6</sup>Isotope Laboratory, Department of Earth and Space Sciences, University of Washington,  
20 Seattle, WA 98195, USA.

21  
22  
23  
24 **Abstract:**

25  
26 Mass-dependent K isotopic fractionations can be used to trace cosmochemical,  
27 geological, and biological processes such as evaporation/condensation, core formation,  
28 magmatic processes, weathering, and cellular metabolism. However, the application of  
29 stable K isotopes has been limited by major isobaric interferences from Ar, common on  
30 conventional multi-collector inductively-coupled-plasma mass-spectrometer (MC-ICP-  
31 MS), particularly for the low-K samples. Here, we present a set of high-precision K  
32 isotopic data acquired on terrestrial rocks, seawater, as well as a lunar meteorite using the  
33 recently released Nu Sapphire™ MC-ICP-MS that utilizes a collision cell to minimize Ar  
34 based interferences while maintaining remarkably high K sensitivity ( $\approx 2000V/ppm$ ). The  
35 influence of several parameters on the precision and accuracy of the K isotopic data has  
36 been evaluated, including total K concentration, K intensity mismatch between sample

1 and standard, HNO<sub>3</sub> molarity mismatch between sample and standard, and the presence  
2 of matrix elements. We found that the Nu Sapphire™ can be used to acquire precise and  
3 accurate data using as little as 125ng of K, which represents an improvement by a factor  
4 10 compared to what has been done on previous instruments. We present data for 23  
5 previously analyzed samples; these data are highly consistent with literature values. On  
6 the other hand, accurate measurements are conditioned 1) to the close matching of sample  
7 and standard K intensities (a 1% mismatch creates a 0.02 ‰ offset on the <sup>41</sup>K/<sup>39</sup>K ratio),  
8 and 2) to the absence of Ca (a Ca/K ratio of 1% creates a 0.069 ‰ offset on the <sup>41</sup>K/<sup>39</sup>K  
9 ratio). In addition, Rb/K, Na/K, Ti/K and Cr/K ratio should also be maintained under  
10 2.5% to avoid isotopic offset.

11 We confirm the existence of significant mass-dependent K isotopic variations in  
12 terrestrial samples and that lunar rocks are isotopically heavier than terrestrial rocks. The  
13 incomparable sensitivity offered by the Nu Sapphire opens the possibility for high-  
14 precision K isotopic measurements across a wide range of samples for diverse  
15 applications.

16

## 1 **Introduction**

2 Potassium is a major or an important minor element in most geological and biological  
3 environments. Potassium is the 20<sup>th</sup> most abundant element in the Sun, and the 17<sup>th</sup> on  
4 Earth (Palme et al., 2014). Due to its incompatible behavior during magmatic processes,  
5 K is highly enriched in the continental crust, which is a major terrestrial reservoir that  
6 contains  $\approx 24\%$  of the total K (Rudnick and Gao, 2003). It is also a highly water-soluble  
7 element and a major cation in seawater (Bruland and Lohan, 2003). In biological systems,  
8 K is fundamental in cell biochemical reactions, energy metabolism, and is essential to  
9 cellular osmotic regulation and the propagation of the nerve impulses through cell  
10 membranes (e.g. Carver, 2019). It is inferred to be one of the light elements in the  
11 terrestrial (Gessmann and Wood, 2002) and lunar (Steenstra et al., 2018) cores due to its  
12 siderophile behavior under high-pressure conditions. Moreover, K is a moderately  
13 volatile lithophile element (temperature of 50 % condensation = 1006 K, Lodders, 2003),  
14 with an abundance that varies greatly between planetary bodies and understanding the  
15 origin of these variations may hold clues to the mechanisms of planetary formation (e.g.  
16 Humayun and Clayton, 1995).

17 Potassium has 2 stable isotopes:  $^{39}\text{K}$  (93.258 %) and  $^{41}\text{K}$  (6.730 %) and a long-  
18 lived radioactive isotope ( $^{40}\text{K}$ ,  $T_{1/2}=1.248\times 10^9$  years, 0.0117 %). In this work, the isotope  
19 composition of K refers to the mass-dependent fractionation of stable isotopes  $^{39}\text{K}$  and  
20  $^{41}\text{K}$ . The difference in the ratio of  $^{41}\text{K}/^{39}\text{K}$  can be used to decipher the different processes  
21 governing the origin of its abundance variations (e.g. evaporation/condensation, core  
22 formation, magmatic processes, weathering, disease affecting it imbalance in the  
23 organism). For example, Wang and Jacobsen (2016) found that the Moon is isotopically

1 heavier in K isotopes compared to the Earth, and suggested that this reflected volatile  
2 events during Moon formation.

3 While potassium is one of the elements with the lowest first ionization potential,  
4  $\approx 4.34$  eV (<https://physics.nist.gov/PhysRefData/ASD/ionEnergy.html>), there have been  
5 relatively limited high precision isotopic studies because of major drawbacks on both  
6 multi-collector thermo-ionization (TIMS) and inductively-coupled plasma (MC-ICP-MS)  
7 mass spectrometers and in-situ measurements by secondary ion mass spectrometers  
8 (SIMS) returned precision of  $\approx 0.5$  ‰ (Humayun and Clayton 1995). Because K has  
9 only 3 natural occurring isotopes, it is not possible to correct for instrumental mass bias  
10 by double spike addition which therefore limits the precision that can be obtained for  
11 stable isotope ratios by TIMS to  $\approx 1$  ‰ at best (e.g. Verbeek and Schreiner, 1967). On the  
12 other hand, MC-ICP-MS has become the instrument of choice to analyze elements with 2  
13 or 3 stable isotopes mostly because of its rapid sample throughput and compatibility with  
14 sample-standard bracketing method for mass bias correction (e.g. Lu, (Blichert-Toft et  
15 al., 1997), Cu (Maréchal et al., 1999)). However, ionization is obtained in an Ar plasma  
16 for conventional MC-ICP-MS, which generates major isobaric interferences as  $^{38}\text{ArH}^+$ ,  
17  $^{40}\text{Ar}^+$  and  $^{40}\text{ArH}^+$  on  $^{39}\text{K}$ ,  $^{40}\text{K}$  and  $^{41}\text{K}$ , respectively, which makes high-precision K  
18 isotopic measurements more cumbersome than for most elements. One approach to  
19 circumvent these problems has been to limit argides generation at a decreased Ar plasma  
20 temperature and to resolve the interferences at an increased mass resolution (e.g. Chen et  
21 al., 2019 ; Hu et al., 2018; Morgan et al., 2018; Tuller-Ross et al., 2019; Xu et al., 2019).  
22 Using this technique,  $^{41}\text{K}/^{39}\text{K}$  reproducibility as precise as  $\approx 50$  ppm (2SE) can be  
23 obtained but it necessitates the use of over 5  $\mu\text{g}$  of K (Chen et al., 2019; Hu et al., 2018 ;

1 Xu et al., 2019). Recently Chen et al. (2020) also achieved a similar precision with a dry  
2 plasma method where an Apex Omega desolvating nebulizer system was used to suppress  
3 the formation of argon hydrides without lowering the RF power. Alternatively, collision  
4 cell MC-ICP-MS, theoretically allows the reduction of the amount of charged argides via  
5 collision and reaction with a neutral or reactive gas. Until recently (Ku and Jacobsen,  
6 2020), only the Micromass Isoprobe, which is an older generation single-focusing MC-  
7 ICP-MS had been equipped with such collision cell. For example, Li et al. (2016)  
8 performed isotopic measurements on a Micromass Isoprobe using D<sub>2</sub> as the collision gas,  
9 and obtained a precision of  $\approx 200$  ppm (2SD) for <sup>41</sup>K/<sup>39</sup>K with a couple of  $\mu\text{g}$  of K  
10 samples being analyzed. A new generation of dual-path MC-ICP-MS with collision cell  
11 capability has been released by Nu Instruments in 2018, known as the Sapphire. It is  
12 promising to obtain high-precision K isotopic data on small samples with this novel  
13 instrument because it is the first MC-ICP-MS to combine state-of-the-art interface, double-  
14 focusing ion optics, and a collision cell, to allow testing the accuracy of the data obtained  
15 using pseudo-high resolution and the older generation collision cell instrument. So far  
16 only one paper reported K isotopic data measured on this instrument (Ku and Jacobsen,  
17 2020); their analyses use  $\approx 1$   $\mu\text{g}$  of K and yield an internal precision (2SE) of 30 ppm and  
18 an external reproducibility (2SD) of 27 ppm over a 9-day period. However, this paper  
19 focused on the potassium isotopic composition of meteorites and report only 5 data for  
20 terrestrial rock geostandards (including seawater). Here we report new data obtained on  
21 23 samples, including a large variety of international geostandards on which data had  
22 been previously acquired by pseudo-high resolution on a Neptune Plus or on a Nu Plasma  
23 II. Furthermore, we report the limitation on the accuracy of the data obtained from

1 various analytical effects such as the effect of Ca (that would produce CaH<sup>+</sup> interference  
2 on <sup>41</sup>K) and on the intensity mismatch between samples and standard.

3

#### 4 **Samples and Methods**

##### 5 **Samples**

6 The samples analyzed here comprise W-1 (diabase, United States Geological Survey,  
7 USGS), JB-1 (basalt, Geological society of Japan, GSJ), SGR-1 (shale, USGS), GSP-1  
8 (granodiorite, USGS), AGV-1 and AGV-2 (andesite, USGS), BHVO-2 (basalt, USGS),  
9 BCR-2 (basalt, USGS), G-2 (granite, USGS), SY-1 and SY-2 (Syenite, Canadian  
10 Certified Reference Materials Project, CCRMP), MAG-1 (marine mud, USGS),  
11 Hawaiian seawater (internal standard, University of Washington), GH (granite, Centre de  
12 Recherches Pétrographiques et Géochimiques, CRPG), GA (granite, CRPG), GBW07111  
13 (granite, National Research Center for Geoanalyses of China, NRCG), GBW07103  
14 (granite, NRCG), FK-N (Feldspar potassium, ANRT), SDC-1 (Mica shist, USGS), QLO-  
15 1 (quartz latite, USGS), DRN (diorite, ANRT), RGM-1 (rhyolite, USGS) and LAP 02224  
16 (lunar meteorite). The Hawaiian seawater is an internal standard from the University of  
17 Washington, but as demonstrated before (Hill et al. 2019, Wang et al. 2020), seawater is  
18 homogeneous regardless of location, depth, or K concentration, and therefore it can be  
19 taken as representative of global seawater. The selected samples cover a range of  
20 chemical compositions and most of them have previously been analyzed for their K  
21 isotopic compositions in multiple laboratories. Therefore, they are well suited to test the  
22 accuracy of the Nu Sapphire measurements, as well as to confirm previous results  
23 obtained on standard MC-ICP-MS. Furthermore, BHVO-2 has been used to evaluate the

1 long-term reproducibility of the method and has been analyzed 11 times over a 6-month  
2 period from three separate dissolutions and chemical purifications (Table S1).

3 To evaluate the effect of the intensity mismatch between sample and standard we  
4 performed tests on a pure K concentration standard (NIST SRM 3141a) as well as on one  
5 geological material (DR-N) running them both with 0 to 10 % intensity mismatch, as  
6 compared to the bracketing standard (NIST SRM3141a). The effect of  $^{40}\text{CaH}^+$   
7 interference on  $^{41}\text{K}$  has also been tested on both the pure K standard and on one  
8 geological material (GH) by adding Ca up to 4%. Finally, we tested the effect of K  
9 concentration on the accuracy of the data from 150 ppb down to 25 ppb of K (which for 5  
10 replicates would represent  $\approx 750$  and  $\approx 125$  ng of K, respectively).

11

## 12 **Dissolution and chemical purification**

13 The chemical purification has been conducted at either the Institut de Physique du  
14 Globe de Paris (IPGP), and University of Washington as described here (Xu et al., 2019)  
15 or at Washington University in St Louis as described in Chen et al. (2019). At  
16 Washington University, all samples were grounded in an agate mortar. 50-100 mg of  
17 powders were dissolved in concentrated HF-HNO<sub>3</sub> following by a second dissolution in  
18 HCl-HNO<sub>3</sub> using Parr sample digestion vessels for both steps. Then samples were dried  
19 down and re-dissolved in 0.7 N HNO<sub>3</sub>. Potassium is purified using a two-step ion  
20 exchange chromatography. The first separation is done on a “big” column (Bio-Rad  
21 Econo-Pac; I.D.=1.5cm) filled with 17 mL of AG50-X8 100–200 mesh cation-exchange  
22 resin. A second purification is done on a “small” column (Bio-Rad glass Econo-column;  
23 I.D.=0.5cm) filled with 2.4 mL of the same resin. Both columns were first cleaned with 6

1 N HCl. Samples in 1 mL of 0.7 N HNO<sub>3</sub> were loaded on the “big” columns. First 87 mL  
2 of 0.7 N of HNO<sub>3</sub> are passed to clean up the matrix. The K fractions were collected by  
3 adding 107 mL of 0.7 N HNO<sub>3</sub>. On the second column, the samples are loaded in 1 mL of  
4 0.5 N HNO<sub>3</sub>. Matrix were eluted using 16 mL 0.5 N HNO<sub>3</sub>. 18 mL of 0.5 N HNO<sub>3</sub> are  
5 then added to collect the K.

6 At IPGP and University of Washington, 20-25 mg pulverized rock standards were  
7 digested sequentially using Optima-grade concentrated HF-HNO<sub>3</sub>, HCl-HNO<sub>3</sub>, and  
8 HNO<sub>3</sub>. The closed beakers were heated on a hotplate at 120°C, periodically vibrated in an  
9 ultrasonic bath, and opened and dried at 100°C. The dried samples were redissolved in  
10 0.5 N HNO<sub>3</sub> in preparation for the cation-exchange chromatography. Potassium was  
11 purified by two passes of 2mL pre-cleaned Bio-Rad AG50W-X8 resin (200-400 mesh)  
12 that was filled in Bio-Rad Poly-Prep polyethylene columns and conditioned by 10 mL 0.5  
13 N HNO<sub>3</sub>. Sample solutions were then loaded on the resin and eluted by 0.5 N HNO<sub>3</sub>.  
14 Matrix elements were eluted with 13 mL of 0.5 N HNO<sub>3</sub>, and K was collected from the  
15 subsequent 22 mL fraction. The resin was cleaned with 10 mL of 6 N HCl afterward.

16 To minimize procedure blank, acid-washed teflon beakers and double-distilled acids were  
17 used exclusively in this study, which were prepared in house at either Washington  
18 University in St Louis, University of Washington, USA, or at IPGP.

19

## 20 **K isotopic measurements on Sapphire**

21

22 Collision cells have been in use with quadrupole ICP-MS for nearly 20 years and  
23 have proven effective to remove Ar based species and other molecular interferences. But  
24 it is also known to create complications for isotope systems due to the mass  
25 discrimination effects of the multipole and inherent instrumental isotopic bias.

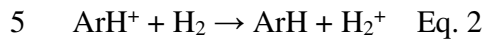
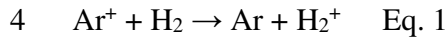


1           The Nu Sapphire features by a dual-path design (Figure 1), including both a  
2 conventional MC-ICP-MS (High Energy, 6 kv acceleration) pathway and a collision cell  
3 (Low Energy, 4 kv acceleration) pathway. This design allows for selecting either classic  
4 or novel applications without compromising the analysis. For K isotope measurements,  
5 we used the collision cell pathway.

6           The Nu Sapphire installed at IPGP is a double-focusing magnetic sector MC-ICP-  
7 MS instrument equipped with 16 fixed Faraday collectors that are fitted with selectable  
8 resistors ranging from  $10^{10}$  to  $10^{13}$  ohm. For the low energy pathway, at the plasma  
9 source, the ions are accelerated at 4kV. The ions are deflected off-axis and decelerated to  
10 a few 10eV's of energy to enter the radio frequency (RF) multipole collision/reaction  
11 cell. The RF hexapole reduces mass bias effects compared to quadrupole-based cells due  
12 to the larger mass transmission window. This is because quadrupoles have the steepest  
13 confining potential, i.e., the potential rises quickly from the center of the device to the  
14 rods, thus permitting operation within a narrow bandwidth as well as operation in other  
15 modes that are highly selective with respect to the mass-to-charge ratio (Amr, 2012).  
16 Hexapoles, on the contrary, are much less selective with respect to the mass-to-charge  
17 ratio, but can provide higher ion transmission and reduced scattering losses.

18           Within the gas filled cell the ions are collisionally thermalized by colliding with  
19 the buffer background gas, and charge exchange takes place with hydrogen, removing the  
20 Ar based species. After the cell, the ions are re-accelerated to 4 kV and focused back onto  
21 the mass spectrometer source slit in the same manner as on a conventional MC-ICP-MS  
22 (or as if it were following the high energy path on the Nu Sapphire).

1           The charge exchange with H<sub>2</sub> gas in the collision/reaction cell reduces the Ar<sup>+</sup>  
2 signal by greater than 9 orders of magnitude, to almost completely remove any Ar based  
3 species, for example:



6

7 In addition to the hydrogen gas required for the reaction, He gas is introduced in the cell  
8 as a buffer gas and contributes to the collisional thermalisation of the ions within the cell  
9 in order to maximise transmission through the hexapole ion guide. The relative amount of  
10 He and H<sub>2</sub> introduced in the cell is optimised to minimise the Ar<sup>+</sup>, ArH<sup>+</sup> and CaH<sup>+</sup>  
11 backgrounds (see Table 1 for the parameters used here).

12           In this study, the K isotope data were acquired on the Sapphire instrument in its  
13 Low Energy mode. A 150 ng/g (ppb) NIST SRM3141a K standard solution and various  
14 samples were introduced into the mass spectrometer using an Apex Omega desolvating  
15 system fitted with a 100 μL/min PFA nebulizer (MicroFlow nebuliser, Elemental  
16 Scientific, Omaha, NE, USA) and with standard Ni dry cones (“dry plasma”). We also  
17 performed comparative test using a cyclonic spray chamber (“wet plasma”). Zoom optics  
18 were used to optimize focusing and peak coincidence.

19           Data was collected in static mode (no peak jump), with <sup>39</sup>K<sup>+</sup> measured in a  
20 Faraday cup (L5) connected to a pre-amplifier fitted with a 10<sup>10</sup>ohm resistor and <sup>41</sup>K<sup>+</sup>  
21 using a 10<sup>11</sup>ohm resistor (L1). The intensity of the mass 40 was monitored on the faraday  
22 cup L3 using a 10<sup>11</sup> ohm resistor. Each analysis consists of a 60-second zero  
23 measurement in 3% HNO<sub>3</sub>, followed by 1 block of 50 cycles with 5 second integrations

1 (Table 1). A 90-120 second wash was performed in 3 % HNO<sub>3</sub> between each standard  
2 and sample analysis and a transfer time of 60 or 90 seconds was applied. Each sample  
3 was measured between 6 and 12 times, bracketed by the NIST-SRM 3141a standard. No  
4 tuning was made once the sequence had begun. The operating parameters of the  
5 instrument are listed in Table 1.

6 In these conditions, the background on the masses 39 and 41 were  
7 approximately 150 mV and 2 V respectively in dry plasma mode and 39 mV and 450  
8 mV in wet plasma mode. The signal on the mass 40 were approximately between 20  
9 and 100 mV in dry plasma mode and 24 and 62 mV in wet plasma mode. For  
10 comparison, the signal for 150 ppb of K returned over 300 V in dry plasma mode and 20  
11 V in wet plasma mode.

12 All the samples and tests have been performed in dry plasma mode. The wet plasma  
13 mode has only been run to compare the precision and intensity of the SRM3141a K  
14 standard solution to previous studies (Chen et al., 2019; Li et al., 2016; Li et al., 2020;  
15 Morgan et al., 2018; Xu et al., 2019). The mass bias was corrected by measuring the  
16 samples alternatively with the NIST SRM3141a K standard solution (standard-sample  
17 bracketing).

18

## 19 **Results and discussion**

20 The K isotopic data for the samples are reported in Table 2. All the data for the  
21 analytical tests and long-term reproducibility are reported in supplementary tables.

22 All the data are reported using the  $\delta^{41}\text{K}$  notation as:

23

1 
$$\delta^{41}\text{K} (\text{‰}) = \left[ \frac{\left(\frac{^{41}\text{K}}{^{39}\text{K}}\right)_{\text{sample}}}{\left(\frac{^{41}\text{K}}{^{39}\text{K}}\right)_{\text{SRM3141a}}} - 1 \right] \times 1000 \quad (3)$$

2

3 The errors are reported as the 2 standard-deviation of the replicated measurements  
4 as well as the 95% confidence interval (see Hu et al. 2018 for details).

### 5 **Accuracy and long-term reproducibility**

6 The accuracy of our analytical protocol is confirmed by 1) self-bracketing pure K  
7 standards that had expected  $\delta^{41}\text{K}$  of zero (Fig. 2), 2) measuring 19 well-characterized  
8 geostandards that were previously analyzed at UW (Table 2) and replicating the chemical  
9 purification of FK-N geostandard and the seawater at IPGP. The  $\delta^{41}\text{K}$  values of these  
10 geostandards obtained on the Nu Sapphire at IPGP are consistent with those measured on  
11 a Nu Plasma II at UW (Table 2). We also fully processed BHVO-2, BCR-2, and AGV-2  
12 at IPGP; their  $\delta^{41}\text{K}$  values agree well literature data (Table 2).

13 The long-term reproducibility of the K isotopic measurement was evaluated by  
14 repeated measurements of BHVO-2 during 11 analytical sessions (where in each session  
15 BHVO-2 was analyzed between 6 and 10 times) over 6 months, on three separate  
16 dissolution and chemical purification (see Table S1). We obtained an average  $\delta^{41}\text{K}$   
17 of  $-0.434 \pm 0.040 \text{ ‰}$  (2SD, n=11), which is consistent with literature values  
18 ( $\delta^{41}\text{K} = -0.411 \pm 0.012 \text{ ‰}$ , Xu et al. 2020). Our results reveal a long-term reproducibility of  
19  $0.040 \text{ ‰}$  (2SD).

### 20 **Comparison of Sapphire with previous methods**

21 Figure 2 illustrates the sensitivity of the double-focusing, dual-path collision cell-  
22 capable Sapphire instrument for K isotopic measurement compared to previous methods

1 using either older generation, single-focusing collision cell MC-ICPMS (Li et al., 2016)  
2 or no collision cell, double-focusing MC-ICPMS in high energy and cold or hot plasma  
3 (Chen et al., 2019 ; Hu et al., 2018; Morgan et al., 2018; Tuller-Ross et al., 2019; Xu et  
4 al., 2019). The sensitivity is reported to reflect a standard at 150 ppb K for each method.  
5 The Sapphire provides the highest reproducibility both in wet and dry plasma mode  
6 compared to any previous method, as well as the highest sensitivity even when only using  
7 the wet plasma compared to high resolution/dry plasma on conventional MC-ICP-MS.  
8 Given the gain in sensitivity by over a factor of 30 when coupled to the Apex Omega we  
9 have decided to perform most of the tests presented below, as well as the measurement of  
10 the natural samples, in these conditions.

#### 11 **Effect of K concentration on accuracy**

12 While all the samples have been analyzed using 150 ppb K ( $\approx 750$  ng of K for 5  
13 replicates), we have performed tests to evaluate the accuracy of the measurements down  
14 to 25 ppb K ( $\approx 125$  ng of K for 5 replicates) (Figure 3). For both the pure K standard  
15 (Figure 3a) and for a rock sample (DR-N, Figure 3b), the accuracy is maintained down to  
16 25 ppb K. For DR-N the value obtained when running 25ppb of K ( $\delta^{41}\text{K} = -0.555 \pm 0.028$   
17  $\%$ ) is consistent with the value obtained at 150 ppb ( $\delta^{41}\text{K} = -0.566 \pm 0.034 \%$ ) as well as  
18 with literature data (shown as the grey bar on Figure 3b,  $\delta^{41}\text{K} = -0.562 \pm 0.025 \%$ , (Xu et  
19 al., 2019)). This method is therefore very promising for analyzing samples with low K  
20 content. For example, the solution at 25 ppb of K of DR-N was run 8 times (i.e. 200 ng of  
21 K) for a precision of 0.028  $\%$  and analyzing it only 5 times (125 ng of K) would provide  
22 similar precision. This is a major gain compared to previous methods that would require  
23 several micrograms of K for similar quality of data.

## 1 **Effect of K concentration mismatch**

2           The effect of intensity mismatch tests was tested by maintaining the NIST-SRM  
3 3141a bracketing standard at 150 ppb of K while varying the concentration of both the  
4 NIST-SRM 3141a K standard measured as a sample (Figure 4a) or the rock sample  
5 (granite GA) from 10 % lower to 10 % higher concentrations. In Figure 4, the variation  
6 of  $\delta^{41}\text{K}$  values is plotted as a function of the ratio between the K concentration of the  
7 sample analyzed (at various concentrations) and of NIST-SRM 3141a analyzed at 150  
8 ppb. Both the pure K standard and granite GA sample show consistent correlation  
9 between measured offset in  $\delta^{41}\text{K}$  and intensity mismatch. The correlation returns a  
10 relationship of  $\delta^{41}\text{K} \approx 2.2 \times \text{K}_{\text{sample}}/\text{K}_{\text{standard}}$  for the pure standard and  $\delta^{41}\text{K} \approx 2.169 -$   
11  $2.656 \times \text{K}_{\text{sample}}/\text{K}_{\text{standard}}$  for granite GA. Therefore, a 1% mismatch creates a  $\approx 0.02$  ‰  
12 isotopic bias, which is presently a clear limitation in the K isotopic measurements using  
13 the Sapphire. It is therefore paramount to analyze the samples with an intensity match  
14 within 1% of the bracketing standard to obtain accurate data on the Sapphire, which is the  
15 protocol used in this study. As shown below, when the intensities match well, the data  
16 obtained on the Sapphire are accurate and precise (<50 ppm). This sensitivity of the  $\delta^{41}\text{K}$   
17 values to the intensity is most likely due to a combination of the hexapole setup and of  
18 the high K background observed on our APEX Omega, over 2 V of K compared to a  
19 signal of > 300 V of K for a 150 ppb solution. The K background therefore represents  $\approx 1$   
20 ppb of K. It should be noted that the effect reported above is relevant to the instrumental  
21 parameters utilized in our study and this may be different for different instrumental  
22 parameters.

## 23 **Effect of matrix elements**

1           The application of standard-sample bracketing method requires column chemistry  
2 to isolate K from the matrix elements; therefore, the instrumental mass bias on pure K  
3 standards can be assumed to represent that on the bracketed samples. Here we tested the  
4 presence of Ca, Na, Rb, Ti, and Cr on the accuracy of K isotopic measurements. The  
5 elution interval of K overlaps significantly with that of Rb and Cr on common cation  
6 exchange resin (e.g., Chen, et al., 2019; Xu et al., 2019), and residual Ti is identified  
7 when using large columns to process low-K samples (Wang and Jacobsen, 2016). While  
8 Na and Ca can be completely separated from K, they are common contaminants in the  
9 environment, and Na potentially forms molecular interference of  $^{23}\text{Na}^{16}\text{O}^+$  at mass 39.  
10 Plastic containers made of polyethylene, polyethylene terephthalate, or polypropylene  
11 typically have high Ca blanks even after repeated acid cleaning. The presence of Ca is  
12 particularly problematic for analysis using the H<sub>2</sub>-fed collision cell, whereby a fraction of  
13 Ca combines with H to produce CaH<sup>+</sup> and create an isobaric interference on  $^{41}\text{K}$ .

14           For Ca-doping test, we added various amounts of Sigma-Aldrich Ca (up to 5 %  
15 Ca) to pure NIST-SRM 3141a K solutions and then measured them against paired pure  
16 NIST-SRM 3141a K solutions at the same K concentration (Figure 5a). All the tests were  
17 performed with 150 ppb of K, i.e. that 1 % Ca corresponds to 1.5 ppb of Ca, which on a  
18 Faraday cup equipped with a 10<sup>11</sup> ohm resistor returned  $\approx 2\text{V}$  of  $^{40}\text{Ca}$ . A similar approach  
19 has been followed to test the effect on a rock sample (granite GH, Figure 5b). The effect  
20 is similar on both the pure K standard and on the sample, where the  $\delta^{41}\text{K}$  correlates with  
21 the Ca/K ratio (%) of the solution analyzed with a slope of 0.069. In other words, a Ca/K  
22 ratio of 1% ( $\approx 2\text{V}$  of  $^{40}\text{Ca}$  in our cases for 1.5 ppb of Ca) would affect the  $\delta^{41}\text{K}$  value by +  
23 0.069 ‰. We therefore suggest that the Ca content in the solution analyzed should always

1 be kept under 0.3 ppb (400mV on  $^{40}\text{Ca}$  in our case). It should be noted that all the  
2 samples reported here (except one) had a  $^{40}\text{Ca}$  intensity similar to the pure NIST-SRM  
3 3141a solution at 150ppb analyzed as bracketing standard ( $\approx 100\text{mV}$ ) and therefore did  
4 not cause any isobaric interferences. The exception is lunar meteorite LAP 02224, for  
5 which  $^{40}\text{Ca}$  has an intensity of  $\approx 1\text{V}$ . This sample is prepared at Washington University in  
6 St Louis using a large column and hence more acids that likely contribute to the high Ca  
7 contents in the purified sample. Giving the relation defined in Figure 5, the presence of  
8 Ca in this sample would cause a potential increase its  $\delta^{41}\text{K}$  by  $\approx 0.034\text{‰}$ . To minimize  
9 Ca contamination, we used Teflon beakers for instrumental analysis.

10 The other elements (Na, Rb, Cr and Ti) are doped with 1%, 2.5%, 5%, and 10%  
11 concentration ratios to that of K (see supplementary tables). These elements produce  
12 smaller matrix effects than Ca. Sodium creates the smallest effect of these four elements  
13 with  $\sim 0.1\text{‰}$  for 10 %, while Na, Rb, and Ti have similar effect  $\sim 0.2\text{‰}$  for 10%. In any  
14 case, the influence of these elements is negligible if the matrix element concentration is  
15 less than 2.5% of that of K. When presented at higher concentrations, Na, Rb, Cr and Ti  
16 all cause a shift of  $\delta^{41}\text{K}$  to lower values (see supplementary table).

### 17 **Effect of K concentration mismatch**

18 We evaluated the effect of the  $\text{HNO}_3$  concentration mismatch between the  
19 samples and the standard on the accuracy of the  $\delta^{41}\text{K}$  as variations in the acid molarity of  
20 the analyzed solution had been shown to affect the mass bias for Fe isotopes (Malinovsky  
21 et al. 2003). Pure NIST-SRM 3141a K solution were dissolved in  $\text{HNO}_3$  at various  
22 concentrations (from 1 % to 5 %) and were analyzed against a NIST-SRM 3141a solution  
23 dissolved in 3 %  $\text{HNO}_3$  (Figure 6). There is a clear correlation ( $R^2=0.95$ ) between the



1  $\delta^{41}\text{K}$  and the mismatch in  $\text{HNO}_3$  concentration. It is therefore important for the accuracy  
2 of the measurements to dilute all the samples and standards with the same acid  
3 concentrations (Malinovsky et al. 2003; Dauphas et al., 2009). For all the samples  
4 analyzed here, samples and standards were prepared from the same bottle of 3 %  $\text{HNO}_3$ .

## 5 **Potassium isotopic variations in terrestrial geostandards and a lunar meteorite**

6 The various samples analyzed here covers a  $\delta^{41}\text{K}$  range of  $\approx 0.6$  ‰, with the  
7 granite GH being the lightest ( $\delta^{41}\text{K} = -0.590 \pm 0.018$  ‰) and the Hawaiian seawater  
8 standard being the heaviest ( $\delta^{41}\text{K} = +0.139 \pm 0.022$  ‰) samples.

9 The data obtained on the Sapphire compare well with previously published data  
10 (see Table 2 and S1 and Figure 7). All samples fall on a slope of 1 line in Figure 7,  
11 indicating the consistency in the absolute values obtained on the Sapphire with both a Nu  
12 Plasma II and a Neptune plus. This consistency also demonstrates the accuracy of the  
13 high-precision data acquired using other instruments from Ku and Jacobsen (2020), Chen  
14 et al. (2019), Tuller-Ross et al. (2019), and Tian et al. (2019). For example, the sample  
15 that was analyzed the most here and in various literatures, the seawater, returns a  
16  $\delta^{41}\text{K} = +0.139 \pm 0.022$  ‰ (n=12), which is in excellent agreement with the most recent  
17 value suggested by Ku and Jacobsen (2020) ( $\delta^{41}\text{K} = +0.168 \pm 0.014$  ‰, n=64), as well as  
18 with previously acquired values with lower precisions :  $\delta^{41}\text{K} = +0.100 \pm 0.305$  ‰, (Wang  
19 and Jacobsen, 2016),  $+0.02 \pm 0.40$  ‰,  $+0.05 \pm 0.70$  ‰,  $+0.12 \pm 0.13$  ‰ (Li et al., 2016),  
20  $0.03 \pm 0.70$  ‰ (Morgan et al., 2018),  $+0.12 \pm 0.07$  ‰ (Wang et al., 2020) and  $+0.14 \pm 0.02$   
21 ‰ (Hille et al., 2019).

1           Furthermore, our data are consistent with the values previously obtained on the  
2 Sapphire at Harvard University (see Table S2), for AGV-1 ( $-0.473 \pm 0.043 \text{ ‰}$   
3 vs  $-0.440 \pm 0.012 \text{ ‰}$ ) and G-2 ( $-0.470 \pm 0.021 \text{ ‰}$  vs  $-0.420 \pm 0.017 \text{ ‰}$ ).

4           The lunar meteorite analyzed here was the only sample that had a  $^{40}\text{Ca}$  signal  
5 higher than the pure K standard (by about 1V, i.e.  $\approx 0.7$  ppb of Ca in the measured  
6 solution). The data obtained on the Sapphire without correcting for the Ca interference ( $-$   
7  $0.021 \pm 0.034 \text{ ‰}$ ) as well as after Ca correction using the relation define above ( $-0.055 \pm$   
8  $0.034 \text{ ‰}$ ) are fairly consistent with the literature value ( $-0.01 \pm 0.03 \text{ ‰}$ , Tian et al., 2020).  
9 Therefore, although the Ca content of the lunar sample is resolvable, the data appears to  
10 confirm the  $\delta^{41}\text{K} \approx -0.02 \text{ ‰}$  of lunar rocks discovered by Wang and Jacobsen (2016) and  
11 later confirmed by Tian et al. (2020). Terrestrial igneous rocks analyzed here and in the  
12 literature are systematically lighter by  $\approx 0.4 \text{ ‰}$  (see Figure 8). The heavy isotope  
13 enrichment of the lunar basalts for K as well as for other volatile elements such as Zn  
14 (e.g., Paniello et al. 2012, Kato et al. 2015), Cl (e.g. Gargano et al. 2020), Ga (Kato and  
15 Moynier 2017), and Rb (Pringle and Moynier 2017) is a strong case of an evaporative  
16 loss of the volatiles from the Moon and of the presence of a transient lunar atmosphere  
17 (Van Kooten et al. 2020).

18           The excellent agreement between the  $\delta^{41}\text{K}$  values obtained on the Sapphire in  
19 IPGP, Paris on a wide range of previously analyzed samples on different instruments as  
20 well as with the two common samples analyzed on the Harvard Sapphire, confirms the  
21 accuracy of the high precision K data for the meteorites reported in Ku and Jacobsen  
22 (2020) and the remarkable systematic isotopic variation between chondritic samples.  
23 Given a factor of 10 improvement in the sensitivity of K isotopic measurements using a

1 Nu Sapphire, this instrument opens up new applications in cosmochemistry such as the  
2 analyses of K-poor samples (e.g. angrite meteorites), meteorite fractions (e.g. chondrules,  
3 CAIs) or very precious samples such as future sample returned mission from asteroids,  
4 the Moon, and Mars.

5

## 6 **Conclusions**

7 We report K isotopic data acquired with a Nu Sapphire dual-path collision cell-  
8 capable MC-ICP-MS connected to an Apex Omega for 23 samples, including seawater,  
9 terrestrial and lunar rocks that all had been previously analyzed for K isotopes by older  
10 generations of mass-spectrometers. We show that K isotopic data acquired using the  
11 collision-cell on the Nu Sapphire are both accurate (by comparing our data to published  
12 values) and precise (2SD of replicated measurements typically around 0.05 ‰). A major  
13 advantage is the high sensitivity of the instrument as the samples can be analyzed in low-  
14 resolution mode ( $\approx 2000\text{V/ppm}$  of K) and accurate data can be obtained at running  
15 concentrations as low as 25 ppb (which for 5 replicates correspond to  $\approx 125$  ng of K). This  
16 represents a remarkable improvement compared to other methods to analyze small or K-  
17 poor samples and will certainly open up new applications. In order to obtain these results,  
18 care needs to be taken to 1) avoid the presence of Ca in the K solution (a Ca/K ratio of  
19 1% create a 0.069 ‰ offset), 2) match the concentration of the sample and of the standard  
20 (a 1% mismatch create a 0.02 ‰ offset, using our instrumental parameters) as well as the  
21 acid molarity of the sample, and 3) well-characterize the instrument behavior and apply  
22 correction functions for K and Ca signals. Controlling these factors, the data reported  
23 here for 23 geostandards are in good agreement with previous studies using Neptune plus

1 or Nu Plasma II instruments. This consistency therefore confirms the accuracy of the data  
2 that can be obtained on the Sapphire in the future.

3

4 Acknowledgements: We thank the two anonymous reviewers for their  
5 constructive reviews that greatly improved the quality of the work. We also thank editor  
6 Balz Kamber for his comments and efficient handling of our manuscript. F. M. thanks the  
7 DIM ACAV+ (Domaine d'Interet Majeur, Astrophysique et Condition d'Apparition de la  
8 Vie) of the region Ile de France for providing part of the funding for the Nu Sapphire.  
9 F.M. acknowledges funding from the European Research Council under the H2020  
10 framework program/ERC Starting Grant Agreement (#637503-PRISTINE) and financial  
11 support of the UnivEarthS Labex program at Sorbonne Paris Cité (#ANR-10-LABX-  
12 0023 and #ANR-11-IDEX-0005-02). Parts of this work were supported by IPGP  
13 multidisciplinary program PARI.

14

15

16

#### 17 **Figure and Table Captions:**

18 **Figure 1.** Sapphire dual path design schematic. The low energy path (blue line) is used to  
19 analyzed K stable isotopes. See main text for details.

20 **Figure 2:** Comparison of the sensitivity of various instruments and techniques used to  
21 analyze the K isotopic composition of a pure K standard at 150ppb. The error bar  
22 represents the 2SD.

23

24 **Figure 3:**  $\delta^{41}\text{K}$  as a function of the K concentration (ppb) for the pure K standard  
25 SRM3141a (Figure 3a) and for the geostandard DR-N (Figure 3b). Measurements are  
26 accurate down to 25ppb.

27

28 **Figure 4:** Effect of the intensity mismatch on the accuracy of the K isotopic composition.  
29 The x-axis represents the ratio of the total intensity of the sample and of the standard. The

1 standard was measured at 150ppb. Figure 4a: Effects on the pure K standard. Figure 4b:  
2 Effects on the GA rock standard.

3  
4 **Figure 5:** Effect of the Ca content of the solution analyzed on the accuracy of the K  
5 isotopic composition. The x-axis represents the Ca content of the solution with regards to  
6 the K concentration (150ppb for all samples) in %. Figure 5a corresponds to the pure  
7 NIST SRM3141a standard and Figure 5b corresponds to the GH rock standard. The slope  
8 is similar in both cases (0.069) and therefore 1% Ca/K ratio biased the  $\delta^{41}\text{K}$  by +0.069  
9 ‰.

10  
11 **Figure 6:** Effect of  $\text{HNO}_3$  concentration mismatch between sample and standard on the  
12  $\delta^{41}\text{K}$  values. The “sample” here represents the pure NIST SRM3141a standard dissolved  
13 in acid at various molarity from 1% to 5%  $\text{HNO}_3$ . The bracketing standard is a pure NIST  
14 SRM3141a solution in 3%  $\text{HNO}_3$ . There is a clear effect of the mismatch of acid molarity  
15 on the accuracy of the  $\delta^{41}\text{K}$ .

16  
17 **Figure 7:**  $\delta^{41}\text{K}$  values from the literature (see Table 2) reported against  $\delta^{41}\text{K}$  values  
18 obtained here on the Nu Sapphire. The dotted line represents a straight line with a slope  
19 1. Most samples fall on the slope 1 line and confirms that the data obtained on the  
20 Sapphire are consistent with literature values.

21  
22 **Figure 8:**  $\delta^{41}\text{K}$  values of the different samples reported here. The lunar basaltic meteorite  
23 (LAP 02224) is isotopically heavier than all terrestrial rocks.

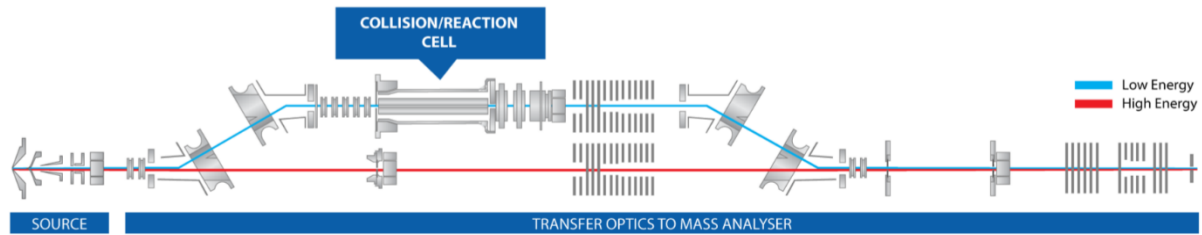
24 **Table 1.** Operating parameters of the Sapphire instrument and the Apex Omega  
25 introduction system.

26 **Table 2:** Potassium isotopic data of the various rock samples analyzed here. The  
27 literature data are all from Xu et al. (2019) except for FK-N (Chen et al., 2019) and LAP  
28 02224 (Tian et al., 2020).

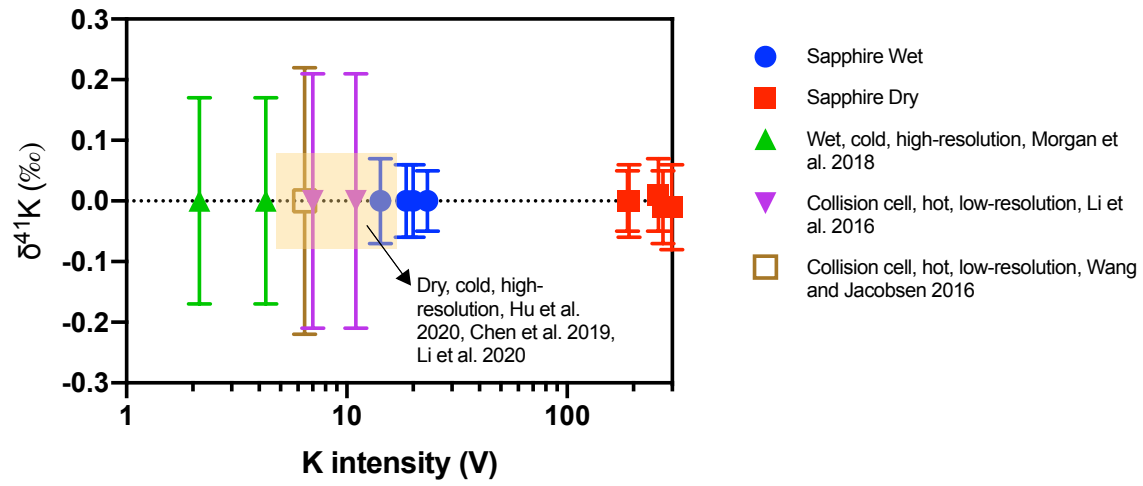
## 1   **References**

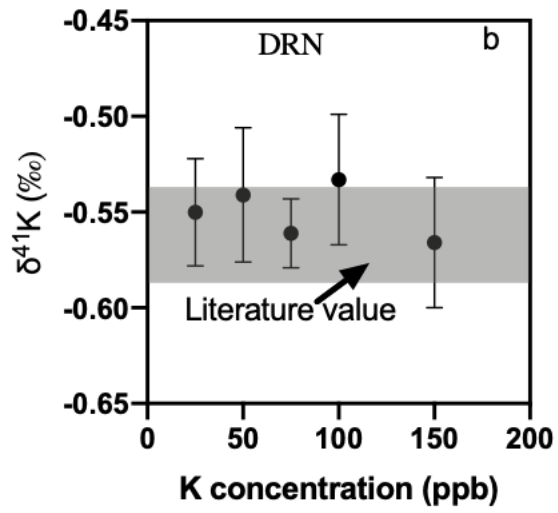
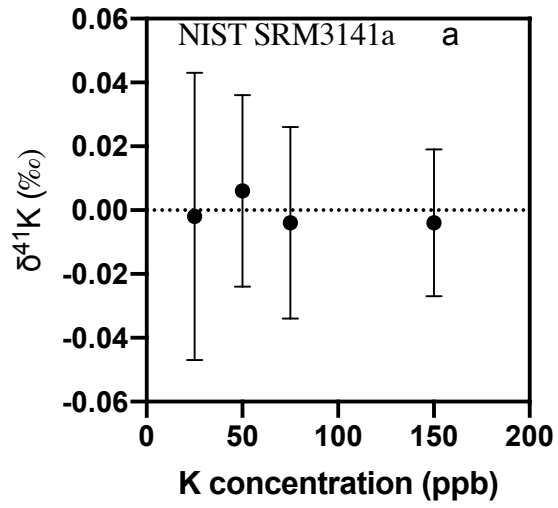
- 2   Amr, M.A., 2012. The collision/reaction cell and its application in inductively coupled  
3        plasma mass spectrometry for the determination of radioisotopes: A literature  
4        review. *Adv. Appl. Sci. Res.* 3, 2179-2191
- 5   Blichert-Toft, J., Chauvel, C., Albarède, F., 1997. Separation of Hf and Lu for high-  
6        precision isotope analysis of rock samples by magnetic sector-multiple collector  
7        ICP-MS. *Contrib. Mineral. Petrol.*, 127: 248-260.
- 8   Bruland, K.W., Lohan, M.C., 2003. The control of trace metals in seawater. In: Holland,  
9        H.D., Turekian, K.K. (Eds.), *Treatise on Geochemistry*. Elsevier.
- 10   Carver, P., 2019. *Essential Metals in Medicine: Therapeutic Use and Toxicity of Metal*  
11        Ions in the Clinic. De Gruyter, Berlin, Germany.
- 12   Chen, H., Tian, Z., Tuller-Ross, B., Korotev, R.L., Wang, K., 2019. High-precision  
13        potassium isotopic analysis by MC-ICP-MS: an inter-laboratory comparison and  
14        refined K atomic weight. *Journal of Analytical Atomic Spectrometry*, 34: 160-  
15        171.
- 16   Chen, H., Liu, X-M., and Wang, K., 2020. Potassium isotope fractionation during  
17        chemical weathering of basalts. *Earth and Planetary Science Letters*, 539, 116192.
- 18   Dauphas, N., Pourmand, A., Teng, F.Z., 2009. Routine isotopic analysis of iron by HR-  
19        MC-ICPMS: How precise and how accurate? *Chemical Geology*, 267: 175-184.
- 20   Gargano, A., Sharp, Z., Shearer, C., Simon, J., Halliday, A., Buckley, W. 2020.  
21        Proceedings of the national academy of sciences. The Cl isotope composition and  
22        halogen contents of Apollo-return samples. 117 (38) 23418-23425
- 23   Gessmann, C., Wood, B., 2002. Potassium in the Earth's core? *Earth and Planetary*  
24        *Science Letters*, 200: 63-78.
- 25   Hille, M., Hu, Y., Huang, T.-Y., Teng, F.-Z., 2019. Homogeneous and heavy potassium  
26        isotopic composition of global oceans. *Science Bulletin*, 64: 1740–1742.
- 27   Hu, Y., Chen, X.-Y., Xu, Y.-K., Teng, F.-Z., 2018. High-precision analysis of potassium  
28        isotopes by HR-MC-ICPMS. *Chemical Geology*, 493: 100-108.
- 29   Humayun, M., Clayton, R.N., 1995. Potassium isotope cosmochemistry: Genetic  
30        implications of volatile element depletion. *Geochimica et Cosmochimica Acta*,  
31        59: 2131-2148.
- 32   Kato, C., Moynier, F., Valdes, MC, Dhaliwal, J., Day, JMD., 2015 Extensive volatile loss  
33        during formation and differentiation of the Moon. *Nature Communications* 6, 1-4.
- 34   Kato, C., Moynier, F., 2017. Gallium isotopic evidence for extensive volatile loss from  
35        the Moon during its formation. *Science Advances* 3, e1700571
- 36   Ku, Y., Jacobsen, S., 2020. Potassium isotope anomalies in meteorites inherited from the  
37        protosolar molecular cloud. *Science Advances*, 6: eabd0511.
- 38   Li, W., Beard, B.L., Li, S., 2016. Precise measurement of stable potassium isotope ratios  
39        using a single focusing collision cell multi-collector ICP-MS. *Journal of*  
40        *Analytical Atomic Spectrometry*, 31: 1023-1029.
- 41   Li, X., Han, G., Zhang, Q., Miao, Z., 2020. An optimal separation method for high-  
42        precision K isotope analysis by using MC-ICP-MS with a dummy bucke. *Journal*  
43        *of Analytical Atomic Spectrometry*, 35: 1330-1339.
- 44   Lodders, K., 2003. Solar System abundances and condensation temperatures of the  
45        elements. *Astrophysical Journal*, 591: 1220-1247.

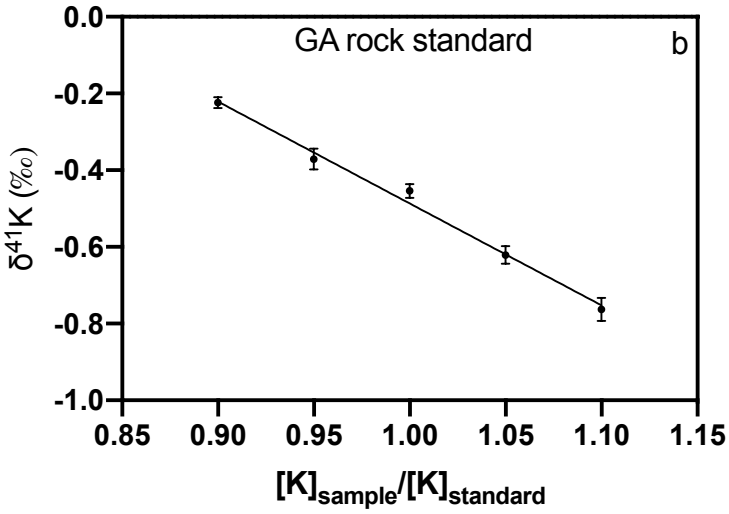
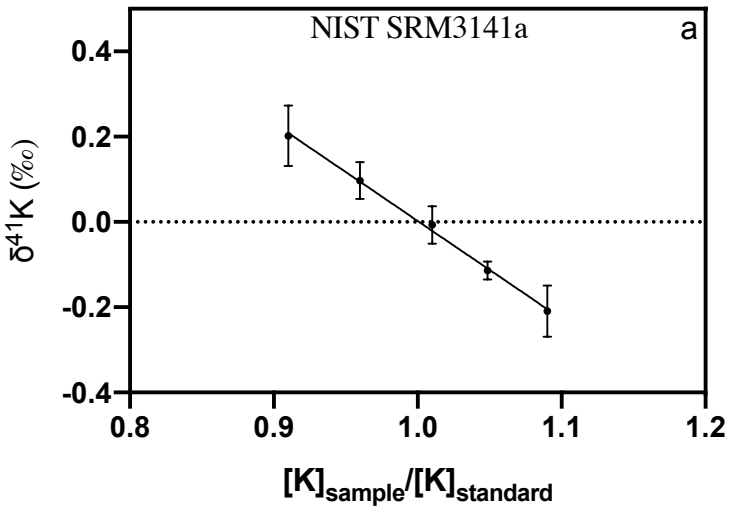
- 1 Malinovsky, D., Stenberg, A., Rodushkin, I., Andren, H., Ingri, J., Ohalnder, B., Baxter,  
2 D., Performance of high resolution MC-ICP-MS for Fe isotope ratio  
3 measurements in sedimentary geological materials. *Journal of Analytical Atomic*  
4 *Spectrometry*, 18: 687-695.
- 5 Maréchal, C., Télouk, P., Albarède, F., 1999. Precise analysis of copper and zinc isotopic  
6 compositions by plasma-source mass spectrometry. *Chem. Geol.*, 156: 251-273.
- 7 Morgan, L.E. et al., 2018. High-precision 41K/39K measurements by MC-ICP-MS  
8 indicate terrestrial variability of  $\delta 41K$ . *Journal of Analytical Atomic*  
9 *Spectrometry*, 33: 175-186.
- 10 Paniello, R., Day, J., Moynier, F., 2012. Zinc isotopic evidence for the origin of the  
11 Moon. *Nature*, 490, 373-376.
- 12 Palme, H., Lodders, K., Jones, A., 2014. Solar System Abundances of the Elements. In:  
13 Holland, H.D., Turekian, K.K. (Eds.), *Treatise in Geochemistry*. Elsevier,  
14 Amsterdam, pp. 41-61.
- 15 Pringle, E., Moynier, F. 2017. Rubidium isotopic composition of the Earth, meteorites,  
16 and the Moon: Evidence for the origin of volatile loss during planetary accretion.  
17 *Earth and Planetary Science Letters*, 473, 62-66.
- 18 Rudnick, R.L., Gao, S., 2003. Composition of the Continental Crust. In: Holland, H.D.,  
19 Turekian, K.K. (Eds.), *Treatise on Geochemistry*, pp. 1-64.
- 20 Steenstra, E. et al., 2018. Depletion of potassium and sodium in mantles of Mars, Moon  
21 and Vesta by core formation. *Scientific Reports* 8: 7053.
- 22 Tian, Z. et al., 2019. Potassium isotopic compositions of howardite-eucrite-diogenite  
23 meteorites. *Geochimica et Cosmochimica Acta*, 266: 611-632.
- 24 Tian, Z. et al., 2020. Potassium isotopic composition of the Moon. *Geochimica et*  
25 *Cosmochimica Acta*, 280: 263-280.
- 26 Tuller-Ross, B. et al., 2019. Potassium isotope systematics of oceanic basalts.  
27 *Geochimica et Cosmochimica Acta*, 259: 144-154.
- 28 Verbeek, A., Schreiner, G., 1967. Variations in 39K: 41K ratio and movement of  
29 potassium in a granite-amphibolite contact region. *Geochimica et Cosmochimica*  
30 *Acta*, 31: 2125-2133.
- 31 Wang, K., Close, H.G., Tuller-Ross, B., Chen, H., 2020. Global average potassium  
32 isotope composition of modern seawater. *Earth and Space Chemistry*, 4: 1010-  
33 1017.
- 34 Wang, K., Jacobsen, S.B., 2016. Potassium isotopic evidence for a high-energy giant  
35 impact origin of the Moon. *Nature*, 538: 487-490.
- 36 Xu, Y.-K. et al., 2019. Potassium isotopic compositions of international geological  
37 reference materials. *Chemical Geology*, 513: 101-107.
- 38

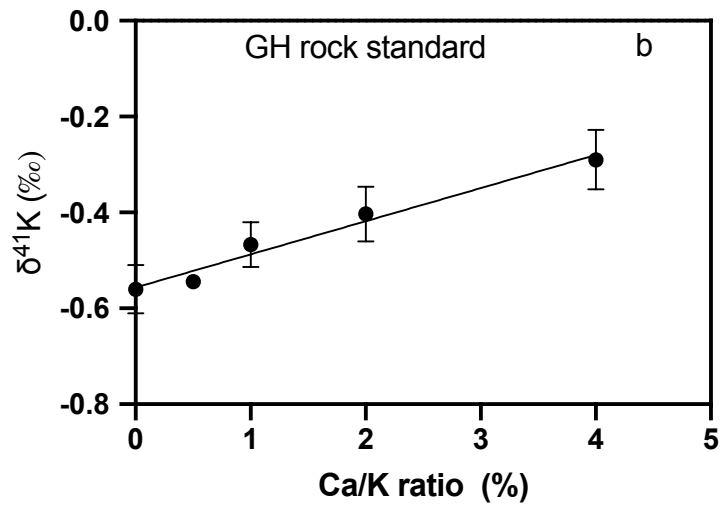
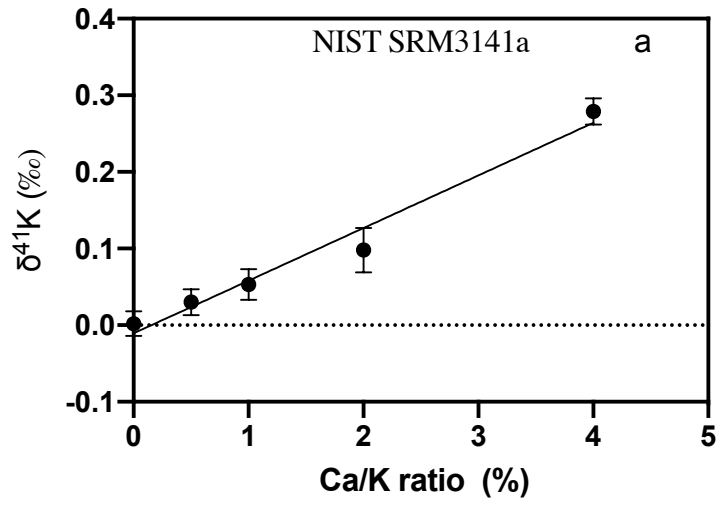


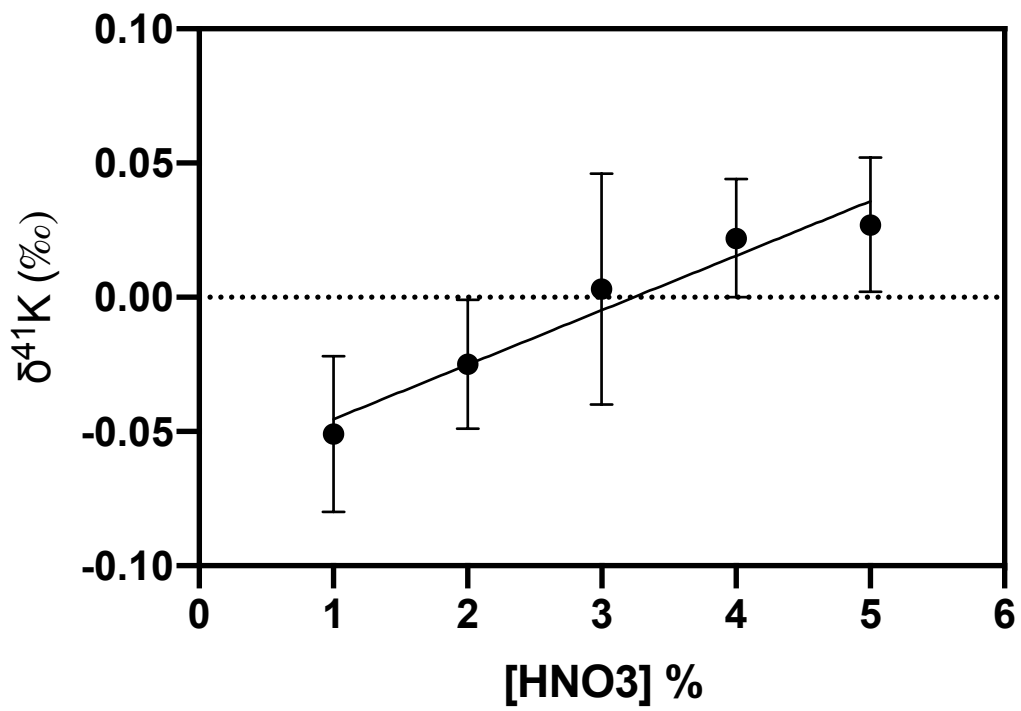


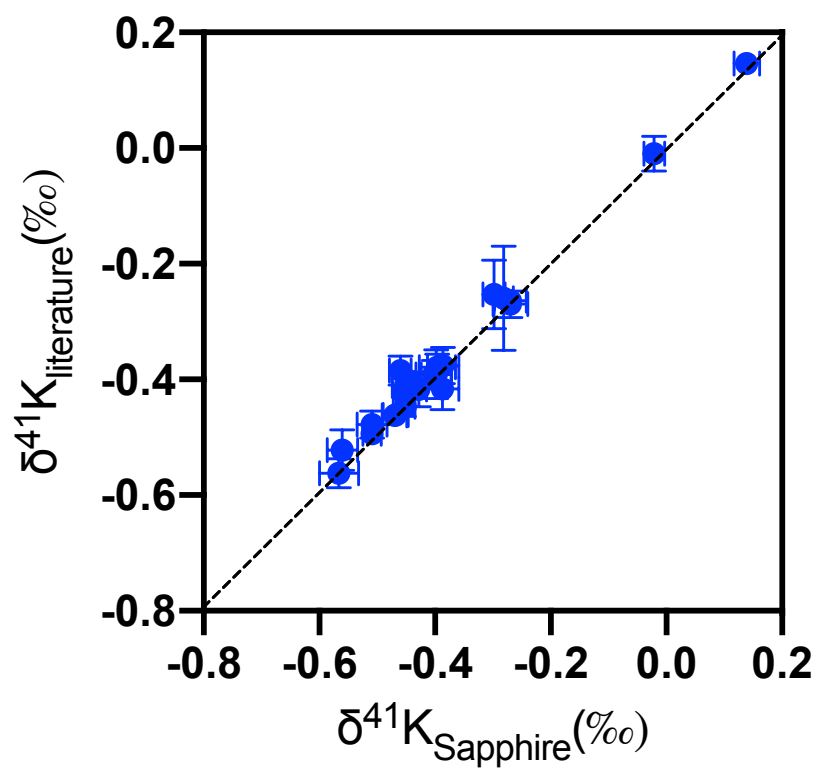


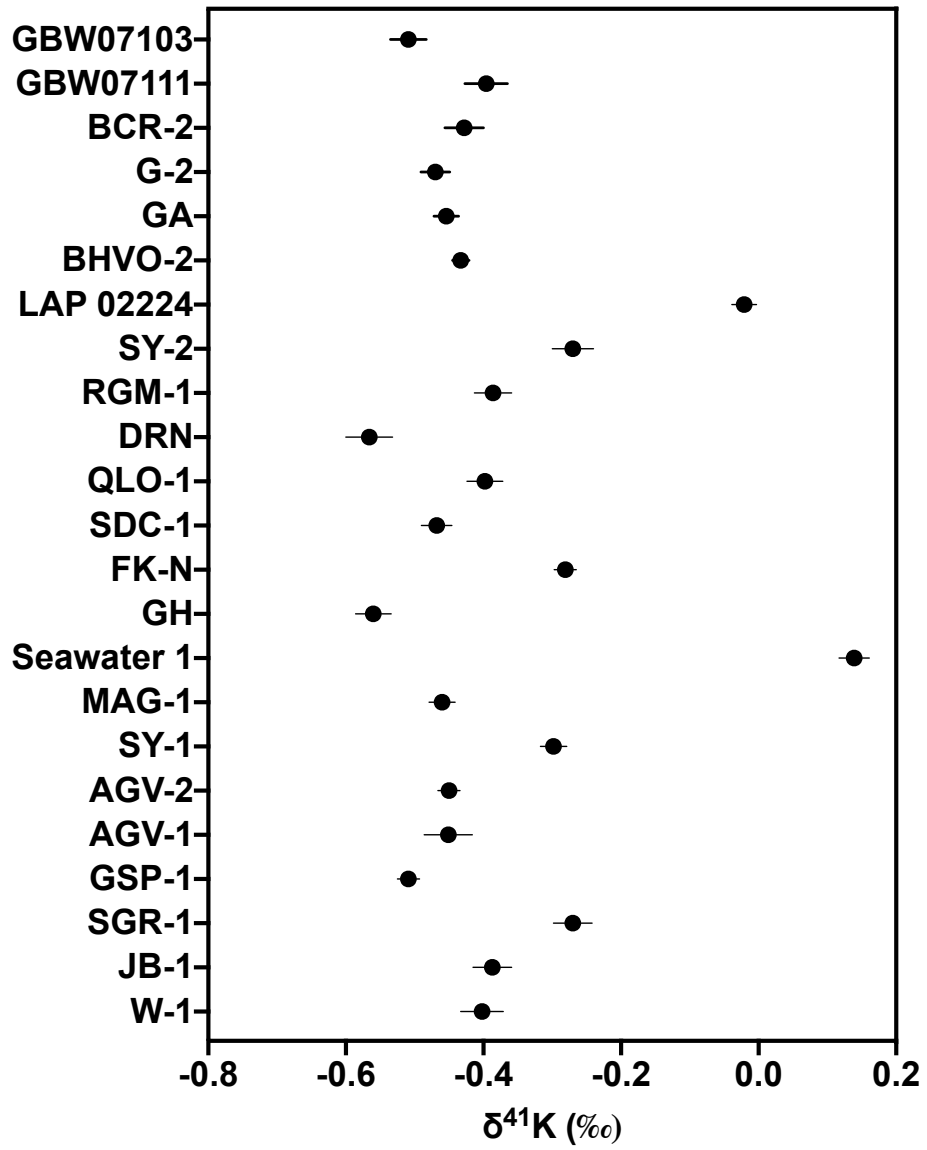












<b>Nu Sapphire Instrument Setting utilized in this study</b>	
RF Power	1300 W
Coolant gas flow rate	13 L/min
Auxiliary gas flow	0.75-0.9 L/min
Sampler/skimmer cone material	Ni
He collision gas flow	2-3 sccm
H <sub>2</sub> reaction gas flow	5 sccm
Quad 1	18.4
Quad 2	-43.0
<b>Apex parameters</b>	
Argon Sweep Gas Flow	2.18-3.42 L/min
Nebulizer pressure	27.4-29.0 psi
Peripump Speed	17.0 (rpm)
Peripump Flow	600.0 (μL/min)
Nebulizer uptake rate	50 or 100 μL/min
Peltier Cooler temperature	3.0 °C
Desolvator temperature	155.0 °C
Spray chamber temperature	140 °C



Sample	Type	$\delta^{41}\text{K}$ (‰)	2SD	95%c.i.	N	$\delta^{41}\text{K}$ (‰) literature	95%c.i.	95%c.i. std	Chemical preparation
W-1	Diabase	-0.402	0.058	0.031	6	-0.391	0.024	0.038	UW
JB-1	Basalt	-0.387	0.053	0.028	6	-0.416	0.036	0.038	UW
BCR-2	Basalt	-0.428	0.028	0.013	7	-0.417	0.030	0.036	IPGP
BHVO-2*	Basalt	-0.434	0.04		11	-0.411	0.011	0.017	IPGP
AGV-1	Andesite	-0.451	0.035	0.016	7	-0.447	0.017	0.027	UW
AGV-2	Andesite	-0.450	0.034	0.016	7	-0.410	0.020	0.033	IPGP
QLO-1	Quartz Latite	-0.398	0.049	0.026	6	-0.391	0.042	0.038	UW
DR-N	Diorite	-0.566	0.066	0.034	6	-0.562	0.025	0.042	UW
GSP-1	Granodiorite	-0.509	0.035	0.016	7	-0.494	0.016	0.036	UW
	duplicate	-0.495	0.058	0.030	6			0.041	UW
GBW07111	Granodiorite	-0.396	0.059	0.031	6	-0.379	0.023	0.044	UW
G-2	Granite	-0.470	0.039	0.021	6	-0.462	0.014	0.040	UW
GH	Granite	-0.560	0.050	0.026	6	-0.522	0.035	0.039	UW
GA	Granite	-0.454	0.034	0.018	6	-0.425	0.023	0.043	UW
GBW07103	Granite	-0.509	0.056	0.026	7	-0.478	0.023	0.038	UW
RGM-1	Rhyolite	-0.386	0.051	0.027	6	-0.376	0.031	0.044	UW
SY-1	Syenite	-0.298	0.046	0.019	8	-0.253	0.059	0.032	UW
SY-2	Syenite	-0.273	0.069	0.032	7	-0.270	0.023	0.038	UW
SGR-1	Shale	-0.270	0.061	0.028	7	-0.264	0.015	0.036	UW
MAG-1	Marine Mud	-0.460	0.037	0.019	6	-0.385	0.025	0.024	UW
SDC-1	Mica Shist	-0.468	0.048	0.022	7	-0.461	0.017	0.033	UW
FK-N	K-Felspar	-0.281	0.031	0.016	6	-0.26	0.09	0.024	UW
FK-N IPGP		-0.303	0.054	0.025	7			0.033	IPGP
Seawater	Water	0.139	0.075	0.024	12	0.146	0.018	0.019	UW
	replicate	0.130	0.070	0.032	7			0.033	UW
LAP 02224	Lunar	-0.021	0.034	0.018	6	-0.01	0.03	0.024	WU

**\*BHVO-2 has been used to estimate the long-term reproducibility evaluated over the course of 11 sessions and three separate chemical procedures (see Table S1 for the details of the measurements).**

